

Effect of kinematic hardening on the initiation and growth of shear bands in plane strain deformations of a thermoviscoplastic solid

Y. M. Wang and R. C. Batra, Rolla, Missouri

(Received March 5, 1992; revised June 24, 1992)

Summary. We study dynamic thermomechanical deformations of an elasto-viscoplastic body deformed in plane strain compression at a nominal strain-rate of 5000 sec^{-1} . The boundaries of the block are assumed to be perfectly insulated. We model the thermoviscoplastic response of the material by the Brown–Kim–Anand constitutive relation in which the evolution of the microstructural changes is accounted for by two internal variables, viz. a scalar and a traceless symmetric second order tensor. The former accounts for the isotropic hardening of the material, and the latter for the kinematic hardening. We model a material defect by introducing a temperature perturbation in the stress-free reference configuration. It is found that the consideration of kinematic hardening does not change the qualitative nature of results.

1 Introduction

Adiabatic shear bands are narrow regions of intense plastic deformation that form during high strain-rate processes, such as shock loading, ballistic penetration, metal forming, and machining. They are called adiabatic since the bands, once they initiate, are fully developed in a few microseconds, and there is not enough time for the heat to be conducted away from the severely deforming region. The primary mode of deformation within the band is that of shearing. Previous numerical [1], [2] and analytical [3] studies have shown that the thermal conductivity affects significantly the band-width. Because of the intense deformations of the material within and surrounding the shear band, the structure of the material changes during the development of the band. One way to account for these structural changes is to use constitutive equations which employ a suitable number of scalar and tensor valued internal variables. Anand [4] has given a set of constitutive equations appropriate for large deformation elasto-viscoplasticity that include two internal variables: a scalar and a symmetric, traceless second-order tensor which, in an average sense, represent an isotropic and an anisotropic resistance to plastic flow offered by the internal state of the material. Brown, Kim, and Anand [5] tested in compression an iron-2% silicon alloy and an 1100-type aluminum alloy at high temperatures and determined the specific forms of the constitutive functionals and the values of material parameters for these alloys. Here we use such a constitutive relation to assess the effect of anisotropic resistance to plastic flow, also known as kinematic hardening, on the initiation and growth of shear bands.

Even though Tresca [6] and Massey [7] observed hot lines, now called shear bands, during the forging of a hot metal in 1878 and 1921, respectively, the research activity in this field picked up since 1944 when Zener and Hollomon [8] observed $32 \mu\text{m}$ wide shear bands during the punching of a hole in a low carbon steel plate. Zener and Hollomon postulated that the heat produced due

to plastic working softened the material, and it became unstable when this thermal softening equalled or exceeded the combined effects of strain and strain-rate hardening. We refer the reader to the review article by Rogers [9], the papers by Shawki and Clifton [10], and Barta and Zhu [11], and a recent issue of Applied Mechanics Reviews [12] for other references on the subject.

2 Formulation of the problem

We use the updated Lagrangian description of motion to describe the thermomechanical deformations of the cylindrical body with square cross-section. That is, to find the deformed shape of the body at time $t + \Delta t$, we take its configuration at time t as the reference configuration. However, the deformations of the body during the time increment Δt need not be small. The governing equations are:

$$\text{Balance of mass} \quad (\rho_r J)^\bullet = 0, \quad (2.1)$$

$$\text{Balance of linear momentum} \quad \rho_r \dot{\mathbf{v}} = \text{Div } \mathbf{T}, \quad (2.2)$$

$$\text{Balance of internal energy} \quad \rho_r \dot{e} = -\text{Div } \mathbf{Q} + \text{tr}(\mathbf{T}\dot{\mathbf{F}}^T), \quad (2.3)$$

where

$$\mathbf{F} = \text{Grad } \mathbf{x} \quad (2.4)$$

is the deformation gradient, $J = \det \mathbf{F}$, \mathbf{x} is the present position of a material particle that occupied place \mathbf{X} in the reference configuration, ρ_r equals the mass density in the reference configuration, \mathbf{v} the velocity of a material particle, a superimposed dot indicates the material time derivative, \mathbf{T} is the first Piola-Kirchhoff stress tensor, the operators Div and Grad signify the divergence and gradient operators applied to field quantities defined on the reference configuration, e is the specific internal energy, and \mathbf{Q} the heat flux per unit undeformed area.

We assume that the material is isotropic, its elastic response can be modeled by Hooke's law, the material moduli are independent of the mass density and the temperature, and the strain-rate tensor \mathbf{D} has additive decomposition into elastic \mathbf{D}^e and plastic \mathbf{D}^p parts. We use the following constitutive relations proposed by Brown, Kim, and Anand [5] for the hot working of metals:

$$\dot{\boldsymbol{\sigma}} - \mathbf{W}\boldsymbol{\sigma} + \boldsymbol{\sigma}\mathbf{W} = \frac{E}{(1+\nu)} \left[(\mathbf{D} - \mathbf{D}^p) + \frac{\nu}{(1-2\nu)} (\text{tr}(\mathbf{D} - \mathbf{D}^p)) \mathbf{I} \right], \quad (2.5)$$

$$\mathbf{D}^p = \frac{3}{2} \frac{\dot{\epsilon}_m^p}{\sigma_m} (\boldsymbol{\sigma}' - \mathbf{B}), \quad (2.6)$$

$$\dot{\epsilon}_m^p = A \exp\left(-\frac{Q}{R\theta}\right) \left[\sinh\left(\xi \frac{\sigma_m}{s}\right) \right]^{1/m}, \quad (2.7)$$

$$\dot{\mathbf{B}} \equiv \dot{\mathbf{B}} - \mathbf{W}\mathbf{B} + \mathbf{B}\mathbf{W} = c_1 \mathbf{D}^p - c_2 \mathbf{B}, \quad \text{tr } \mathbf{B} = 0, \quad (2.8.1-2)$$

$$\dot{s} = \left[h_0 \left| 1 - \frac{s}{s^*} \right|^a \text{sign}\left(1 - \frac{s}{s^*}\right) \right] \dot{\epsilon}_m^p, \quad (2.9)$$

$$s^* = \tilde{s} \left[\frac{\dot{\epsilon}_m^p}{A} \exp\left(\frac{Q}{R\theta}\right) \right]^n, \quad (2.10)$$

$$\mathbf{q} = -k \text{grad } \theta, \quad (2.11)$$

$$\dot{e} = c\dot{\theta} + \text{tr}(\boldsymbol{\sigma}(\mathbf{D} - \mathbf{D}^p)), \quad (2.12)$$

where

$$2\mathbf{D} = \text{grad } \mathbf{v} + (\text{grad } \mathbf{v})^T, \quad 2\mathbf{W} = \text{grad } \mathbf{v} - (\text{grad } \mathbf{v})^T, \quad (2.13.1-2)$$

$$\boldsymbol{\sigma} = J^{-1} \mathbf{T} \mathbf{F}^T, \quad \mathbf{Q} = J \mathbf{F}^{-1} \mathbf{q}, \quad \sigma_m^2 = \frac{3}{2} \text{tr} ((\boldsymbol{\sigma}' - \mathbf{B})^2), \quad (2.14)$$

$$\boldsymbol{\sigma}' = \boldsymbol{\sigma} - \frac{1}{3} (\text{tr } \boldsymbol{\sigma}) \mathbf{I}. \quad (2.15)$$

Equation (2.5) is Hooke's law written in the rate form, $\boldsymbol{\sigma}$ is the Cauchy stress tensor, \mathbf{W} defined by (2.13.2) is the spin tensor, E and ν equal, respectively, the Young's modulus, and Poisson's ratio, the scalar s and the traceless second-order tensor \mathbf{B} are the internal variables that describe the isotropic and kinematic hardening of the material, A is called the pre-exponential factor, Q the activation energy, θ equals the absolute temperature of a material point, R the gas constant, m the strain-rate sensitivity parameter, h_0 a constant rate of athermal hardening, s^* equals the saturation value of s associated with a given temperature/strain-rate pair, and k is the thermal conductivity. The left-hand sides of Eqs. (2.5) and (2.8) equal, respectively, the Jaumann rate of $\boldsymbol{\sigma}$ and \mathbf{B} . In order to characterize the thermoviscoplastic response of the material, we need to specify E , ν , α , A , Q , R , ζ , m , c_1 , c_2 , h_0 , a , \tilde{s} , n , c , and k .

We presume that the plane strain state of deformation prevails, and that the deformations are symmetrical about the horizontal and vertical centroidal axes. Thus, we analyze deformations of the material in the first quadrant and apply the following conditions on the bounding surfaces (see Fig. 1)

$$v_1 = 0, \quad T_{21} = 0, \quad Q_1 = 0 \quad \text{at} \quad x_1 = X_1 = 0, \quad (2.16)$$

$$v_2 = 0, \quad T_{12} = 0, \quad Q_2 = 0 \quad \text{at} \quad x_2 = X_2 = 0, \quad (2.17)$$

$$T_{i\alpha} N_\alpha = 0, \quad Q_\alpha N_\alpha = 0 \quad \text{on the right surface}, \quad (2.18)$$

$$v_2 = -U(t), \quad T_{12} = 0, \quad Q_2 = 0 \quad \text{on the top surface}, \quad (2.19)$$

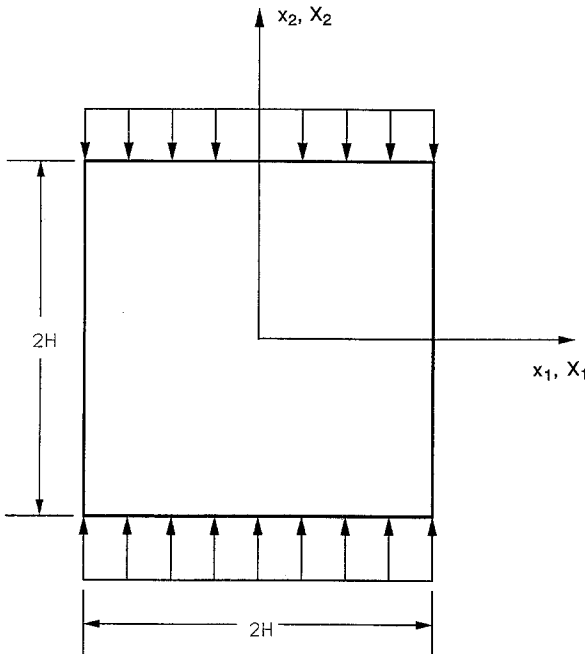


Fig. 1. Schematic sketch of the problem studied

where

$$U(t) = \begin{cases} v_0 t/t_r, & 0 \leq t \leq t_r, \\ v_0, & t \geq t_r. \end{cases} \quad (2.20)$$

That is, all bounding surfaces are thermally insulated, the right surface is traction free, conditions due to the assumed symmetry of deformations apply on the left and bottom surfaces, and on the top surface zero tangential tractions, and a time dependent vertical component of velocity is prescribed. Thus, the contact between the loading device and the upper surface of the body is assumed to be smooth. The assigned vertical velocity on the top surface increases from zero to the steady value v_0 in time t_r .

For the initial conditions we take

$$\begin{aligned} \varrho(\mathbf{X}, 0) &= \varrho_0, & \mathbf{v}(\mathbf{X}, 0) &= \mathbf{0}, & \boldsymbol{\sigma}(\mathbf{X}, 0) &= \mathbf{0}, & \mathbf{B}(\mathbf{X}, 0) &= \mathbf{0}, & s(\mathbf{X}, 0) &= s_0, \\ \theta(\mathbf{X}, 0) &= \theta_0 + \delta \left(1 - \frac{r^2}{2}\right)^{18} \exp(-5r^2), & r^2 &= X_1^2 + X_2^2. \end{aligned} \quad (2.21)$$

These imply that the body is initially at rest, is stress free, has a uniform mass density, and a nonuniform temperature distribution. The initial temperature is higher in a small region around the origin; the magnitude δ of the perturbation signifies, in some sense, the strength of the material defect.

We note that there is no yield or loading surface assumed in our work, and the constitutive relations employed fall in the category of “unified theories of viscoplasticity”. A material point is presumed to undergo elastic deformations at all times. The constraint $\text{tr } \mathbf{B} = 0$ does not require any special consideration since it is satisfied at time $t = 0$ because of the initial conditions, and Eqs. (2.6) and (2.8) give $\text{tr } \dot{\mathbf{B}}(\cdot, 0) = 0$. Thus, $\text{tr } \mathbf{B}(\cdot, t) = 0$ for every t .

3 Computational considerations

The stiff coupled nonlinear equations (2.1)–(2.3), (2.5), (2.8), and (2.9) are to be solved for ϱ , \mathbf{v} , θ , $\boldsymbol{\sigma}$, \mathbf{B} , and s . Since ε_m^p appears only as $\dot{\varepsilon}_m^p$ in Eqs. (2.6), (2.9), and (2.10), we substituted for it from Eq. (2.7), and thus did not take it as one of the variables to be solved for. It is extremely difficult, if not impossible, to prove the existence and/or uniqueness of their solution under the prescribed initial and boundary conditions. Here we seek their approximate solution by the finite element method. A set of nonlinear coupled stiff ordinary differential equations is derived from (2.1)–(2.3), (2.5), (2.8), and (2.9) by using the Galerkin method, and are then integrated with respect to time by using the backward difference Adam’s method included in the subroutine LSODE developed by Hindmarsh [13]. The subroutine adjusts the time step size adaptively to compute a solution of the ordinary differential equations within the prescribed tolerance. The parameters RTOL and ATOL which control the relative and absolute tolerance in the solution variables were each set equal to 10^{-7} . The coordinates of nodes in the finite element mesh were updated after each time step.

4 Computation and discussion of results

In order to compute numerical results, we assigned the following values to various geometric and material parameters:

$$\begin{aligned}
 \rho_0 &= 7860 \text{ kg m}^{-3}, & E &= 168 \text{ GPa}, & \nu &= 0.3, & \mu &= 64.6 \text{ GPa}, \\
 A &= 6.346 \times 10^{15} \text{ sec}^{-1}, & Q &= 100 \text{ KJ mole}^{-1}, & R &= 8.3145 \text{ J mole}^{-1} \text{ }^\circ\text{K}^{-1}, \\
 c &= 473 \text{ J kg}^{-1} \text{ }^\circ\text{C}^{-1}, & k &= 49.22 \text{ W m}^{-1} \text{ }^\circ\text{C}^{-1}, & \bar{s} &= 405 \text{ MPa}, \\
 \theta_0 &= 25 \text{ }^\circ\text{C}, & \delta &= 25 \text{ }^\circ\text{C}, & m &= 1.0, & a &= 1.5, \\
 \xi &= 3.25, & h_0 &= 5000 \text{ MPa}, & H &= 5 \text{ mm}, \\
 v_0 &= 25 \text{ m sec}^{-1}, & t_r &= 10^{-6} \text{ sec}.
 \end{aligned} \tag{4.1}$$

Thus, the nominal strain-rate equals 5000 sec^{-1} and the prescribed speed on the top surface increases from zero to the steady value of 25 m sec^{-1} in one microsecond. In order to study the effect of isotropic and kinematic hardening on the development of the shear band, we studied the following seven different cases.

Case 1: $c_1 = c_2 = 0, \quad n = 0.002.$

Case 2: $c_1 = c_2 = 0, \quad n = 0.05.$

Case 3: $c_1 = 2(10^{-2}) \mu, \quad c_2 = 0, \quad n = 0.002.$

Case 4: $c_1 = 10^{-2} \mu, \quad c_2 = 0, \quad n = 0.002.$

Case 5: $c_1 = 2(10^{-2}) \mu, \quad c_2 = 5(10^5) \text{ sec}^{-1}, \quad n = 0.002.$

Case 6: $c_1 = 10^{-2} \mu, \quad c_2 = 10^5 \text{ sec}^{-1}, \quad n = 0.002.$

Case 7: $c_1 = 10^{-2} \mu, \quad c_2 = 2(10^5) \text{ sec}^{-1}, \quad n = 0.002.$

There is no kinematic hardening for the first two cases, and a comparison of results for them should delineate the effect of the saturation value s^* of s . Results for the other five problems should help illustrate the relative significance of the two terms on the right-hand side of Eq. (2.8.1), giving the evolution of \mathbf{B} , on the development of the shear band. Jayachandran and Batra [14] studied the effect of various parameters in the constitutive relations on the response of the defect free body deformed in plane strain compression and found that an increase in the value of h_0, n, m, \bar{s} , and Q enhances the hardening of the material, and an increase in the value of ξ, a , and A furthers the softening of the material. However, they neither considered kinematic hardening nor studied the nucleation and growth of a shear band.

In the results presented below, a fixed mesh consisting of 32×32 four-noded quadrilateral elements was used, and all integrals defined on an element were evaluated by using the 2×2 quadrature rule. The elements are squares in the initial stress-free configuration, but are quadrilateral for subsequent times because of their unequal deformations in the horizontal and vertical directions. Results computed with a 64×64 mesh of four-noded quadrilateral elements agreed qualitatively with those obtained with the 32×32 mesh, the quantitative difference between the values of temperature at the origin was less than 5% during the entire process of the development of the band. This was not viewed as critical, and because of the considerable savings

in the CPU time resulting from the use of the 32×32 mesh, it was employed for all of the seven cases.

Below we present and discuss results in terms of the following nondimensional variables indicated by a superimposed bar

$$\bar{x} = x/H, \quad \bar{X} = X/H, \quad \bar{v} = v/v_0, \quad \bar{\sigma} = \sigma/\bar{s}, \quad \bar{B} = B/\bar{s}, \quad \bar{\theta} = \frac{\theta}{\theta_0}, \quad \bar{t} = tv_0/H. \quad (4.2)$$

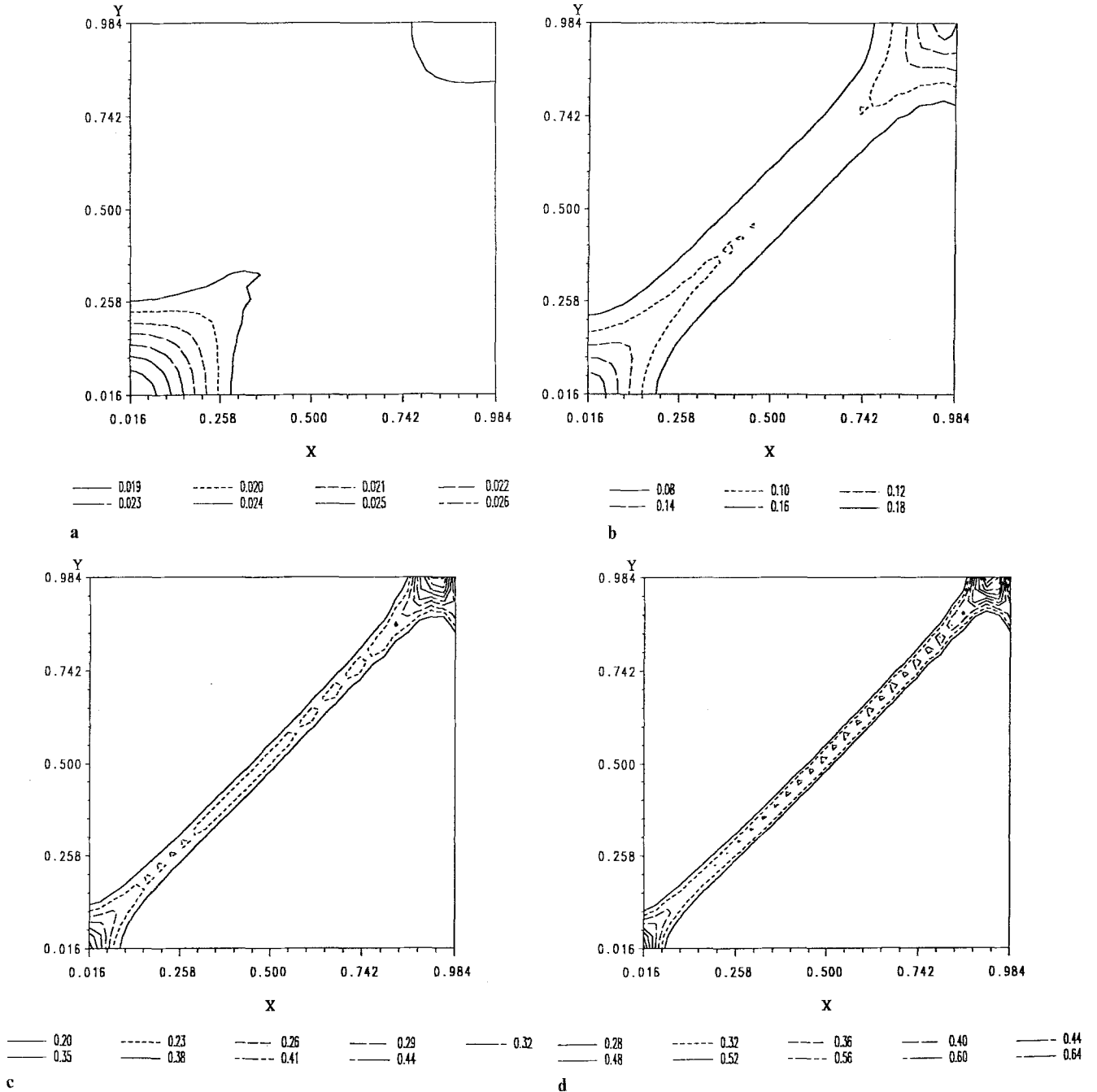


Fig. 2. Contours of the maximum principal logarithmic strain at four different values of the average strain.
a $\gamma_{\text{avg}} = 0.0175$, **b** $\gamma_{\text{avg}} = 0.0576$, **c** $\gamma_{\text{avg}} = 0.0776$, **d** $\gamma_{\text{avg}} = 0.0889$

Here $2H$ equals the height of the block. Henceforth, we use only nondimensional variables and drop the superimposed bar. Because the prescribed downward speed on the top surface increases from zero to one in time t_r , the average strain is slightly less than the nondimensional time.

Figure 2 depicts, in the reference configuration, the contours of the maximum principal logarithmic strain ε , defined as

$$\varepsilon = \ln \lambda, \quad (4.3)$$

where λ^2 equals the maximum eigenvalue of the right ($\mathbf{F}^T\mathbf{F}$) or the left ($\mathbf{F}\mathbf{F}^T$) Cauchy-Green tensor, at four different values of the average strain (γ_{avg}) for case 6. Unless otherwise noted, the results presented below are for case 6; the results for other cases are qualitatively similar to those presented herein. The contours of the maximum principal logarithmic strain suggest that a small region surrounding the center of the cross-section undergoes severe deformations, and these intense deformations propagate along the main diagonal. The severely deforming region progressively narrows down. The reason the domain extends from 0.016 to 0.984 and not from 0.0 to 1.0 in the horizontal and vertical directions is that the X_1 - or X_2 -coordinate of the quadrature point nearest to the left or right and bottom or top surfaces is 0.016 and 0.984. The software used to plot the contours interpolates the data at numerous points from that provided at the quadrature points. We note that the results reported herein are qualitatively similar to those obtained by Zhu and Batra [14] who used a different constitutive relation and did not consider kinematic hardening. By finding the distance through which the contour of $\varepsilon = 0.35$ had travelled from $t = 0.08$ to 0.09125, its average speed of propagation was found to be 208 m/sec. This speed depends upon the state of deformation of the material within the band and also upon the constitutive relation employed. The contours of temperature resemble those of the maximum principal logarithmic strain and are not shown here.

We have plotted in Fig. 3 the variation of the velocity in the x_1 - and x_2 -directions at $\gamma_{\text{avg}} = 0.0889$. It is clear that the body is divided into two deforming triangular regions, one adjoining the top surface that is moving downward at the prescribed speed, and the other abutting the horizontal centroidal plane. These two domains are connected by a narrow transitional region in which the speed in the vertical direction increases sharply from essentially zero to nearly 1.0. The thickness of this transitional layer, which is related to the band-width, equals two elements for the mesh used herein. A finer mesh will probably result in even sharper gradients of the speed within this transition zone. This significant change of speed across the thin transitional layer supports the assertions of Tresca [6] and Massey [7] that the tangential velocity is discontinuous across the shear band. In our work, the velocity field is forced to be continuous within an element and across interelement boundaries. Therefore, jumps in the tangential velocity across a shear band cannot be delineated.

The distribution at $\gamma_{\text{avg}} = 0.0889$ of the effective stress σ_e , defined as

$$\sigma_e^2 = \frac{3}{2} \text{tr} (\boldsymbol{\sigma}' - \mathbf{B})^2, \quad (4.4)$$

and the effective back-stress B_e given by

$$B_e^2 = \frac{3}{2} \text{tr} (\mathbf{B}^2) \quad (4.5)$$

within the block is exhibited in Fig. 4. As expected, the effective stress within the shear band drops. However, the drop is not as precipitous as that found by Batra and Liu [15] who modeled

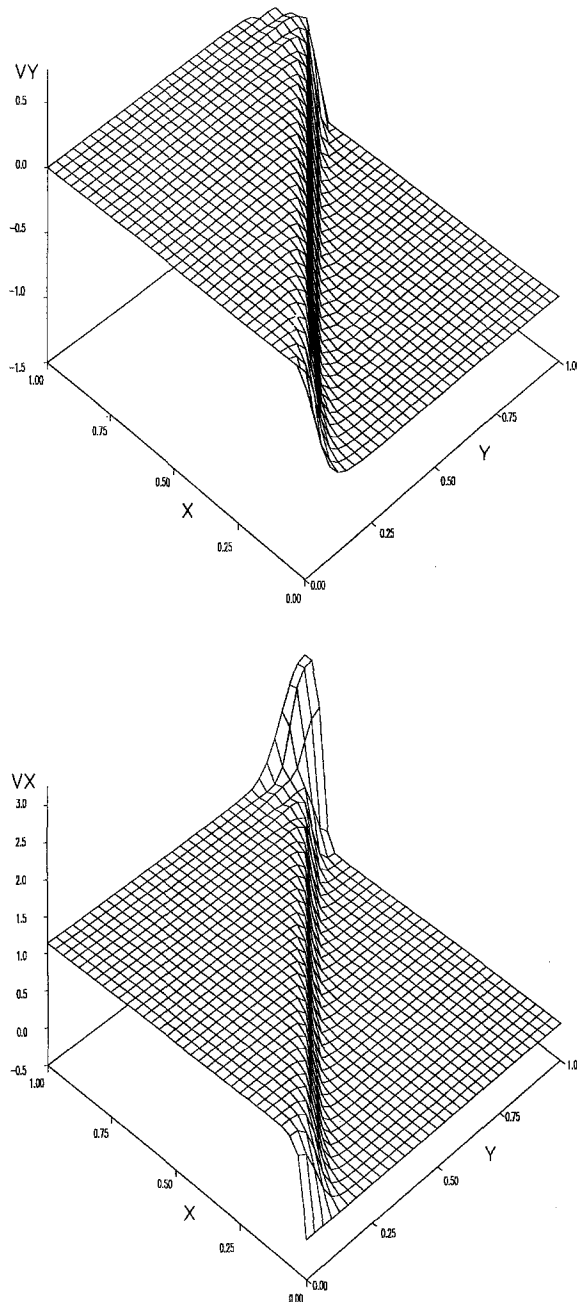


Fig. 3. Distribution of the x_1 - and x_2 -components of the velocity within the deforming region at $\gamma_{\text{avg}} = 0.0889$

thermal softening by an affine function of temperature and assumed a rather large value of the thermal softening coefficient. Zhu and Batra [14] assumed an exponentially decaying softening function and obtained results somewhat similar to that shown here. The effective back-stress B_e within the band is more than that elsewhere in the body, which is consistent with the assumption that the rate of evolution of the back-stress is proportional to the plastic strain-rate. The plastic strain-rate is high at points within the band, and is negligible elsewhere.

The deformed mesh at $\gamma_{\text{avg}} = 0.0889$ plotted in Fig. 5 vividly illustrates that the two elements within the band are significantly deformed and the rest of the body has undergone very little distortion. From results presented thus far, we estimate that at time $t = 0.09$ a large segment of

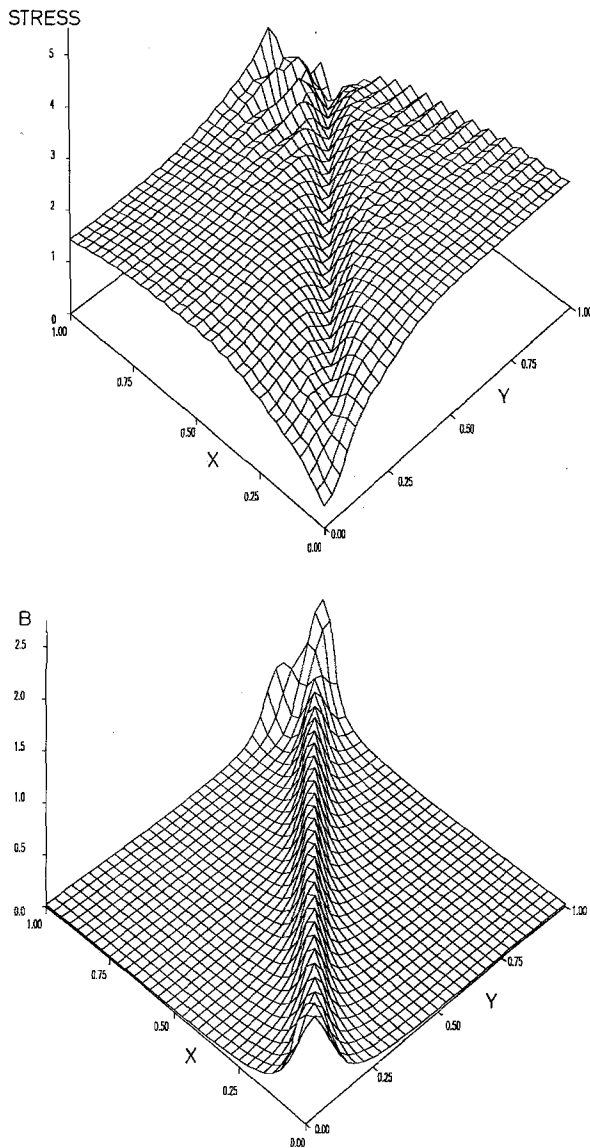


Fig. 4. Distribution of the effective stress and the effective back-stress within the deforming region at $\gamma_{avg} = 0.0889$

the band in the deformed configuration is directed along the line EF that makes an angle of 43° with the horizontal. The orientation of the band changes a little with time. The distribution of the maximum principal logarithmic strain and temperature within the band at different times is exhibited in Fig. 6. These curves reveal that the strain and temperature distributions within the band are nonuniform; the strain and the temperature assume their highest values near the origin and fall off rather rapidly with the distance from O along OEF . In order to decipher the variation of the strain, temperature, effective back-stress, and the rate of dissipation of the energy density defined as $\text{tr}(\sigma D^p)$ across the band, we have plotted, in Figs. 7 and 8, the distribution of these on lines PQ and RS perpendicular to the estimated centerline of the band; these lines are shown in Fig. 7. The abscissa equals the distance from the band centerline of a point along line PQ or RS , and is assigned negative values for points lying above OEF . These plots provide evidence that a narrow band forms around OEF . A finer mesh would probably have resulted in a smoother variation of the strain along PQ and RS , and also in a narrower band. Because of the rather small

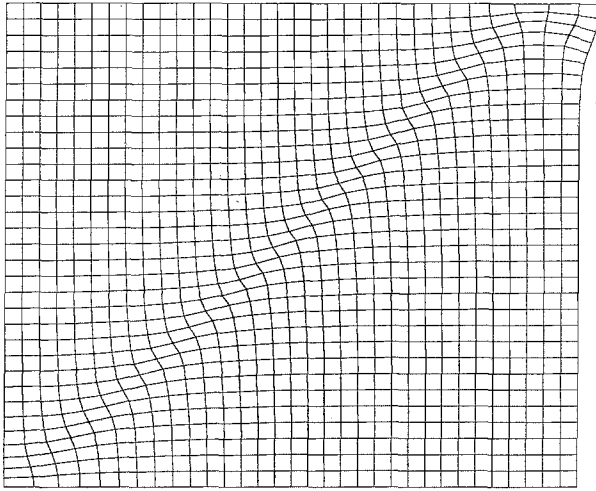


Fig. 5. Deformed mesh at $\gamma_{\text{avg}} = 0.0889$

value of the thermal conductivity, the energy dissipation rate can be regarded as being proportional to the rate of change of temperature. Thus, the temperature changes rapidly at points within the band and slowly at material points outside of it. The energy dissipation rate is a little lower at $t = 0.09$ than that at $t = 0.08$ because of the drop in the value of σ caused by increased thermal softening of the material.

Figure 9 shows the evolution of the maximum principal logarithmic strain, the temperature, the effective back-stress, and the rate of dissipation of the energy density at or near the centroid of the cross-section for four different cases, viz. cases 1, 4, 6, and 7. We note that for case 1 the back-stress always stays at zero. For case 4 the evolution of the back-stress \mathbf{B} is proportional to D^p , and for cases 5 through 7, the present value of the back-stress retards the evolution of \mathbf{B} . The value of c_2 multiplying \mathbf{B} in its evolution equation in case 7 is twice that for case 6. If the rapid increase of the maximum principal logarithmic strain at $X_1 = X_2 = 0.0066$ is taken as the criterion to decide when a shear band initiates, then the shear band is delayed by the consideration of the back-stress. An increase in the value of c_2 results in the band forming a little sooner. For the average strain-rate of 5000 sec^{-1} considered herein, the nondimensional time of 0.10 equals 20 microseconds. The evolution of the temperature at the origin is affected less by the consideration of the back-stress and the values assigned to c_1 and c_2 in the evolution equation for \mathbf{B} . Whereas the temperature vs. average strain curves are concave upward for the problems studied herein, those obtained by Zhu and Batra [14] were concave downward. In both cases, the values of the thermal conductivity and the specific heat were the same. It seems that the curvature of the temperature vs. average strain curve depends upon the way a material defect is modeled. Zhu and Batra [14] considered a rigid non-heat-conducting thin ellipsoidal inclusion, which resulted in a severe stress concentration near the inclusion tips, and the temperature there increased sharply in the beginning and slowly afterward. As expected, the back-stress is highest for case 4 and least for case 1 at any instant of time. For each of the four cases for which results are plotted in Fig. 9, the energy dissipation rate attains a peak value at time $t \cong 0.075$, the rate for the no back-stress case being always higher than that for the other three cases. Thus, the rate of increase of temperature at the origin will decrease for $t \geq 0.075$. This is not transparent from the plots of the evolution of the temperature, mainly because of the scale used.

We have plotted in Fig. 10 the load displacement curves for cases 1, 4, 6 and 7, both with and without the initial temperature perturbation. Since the nondimensional height of half of the

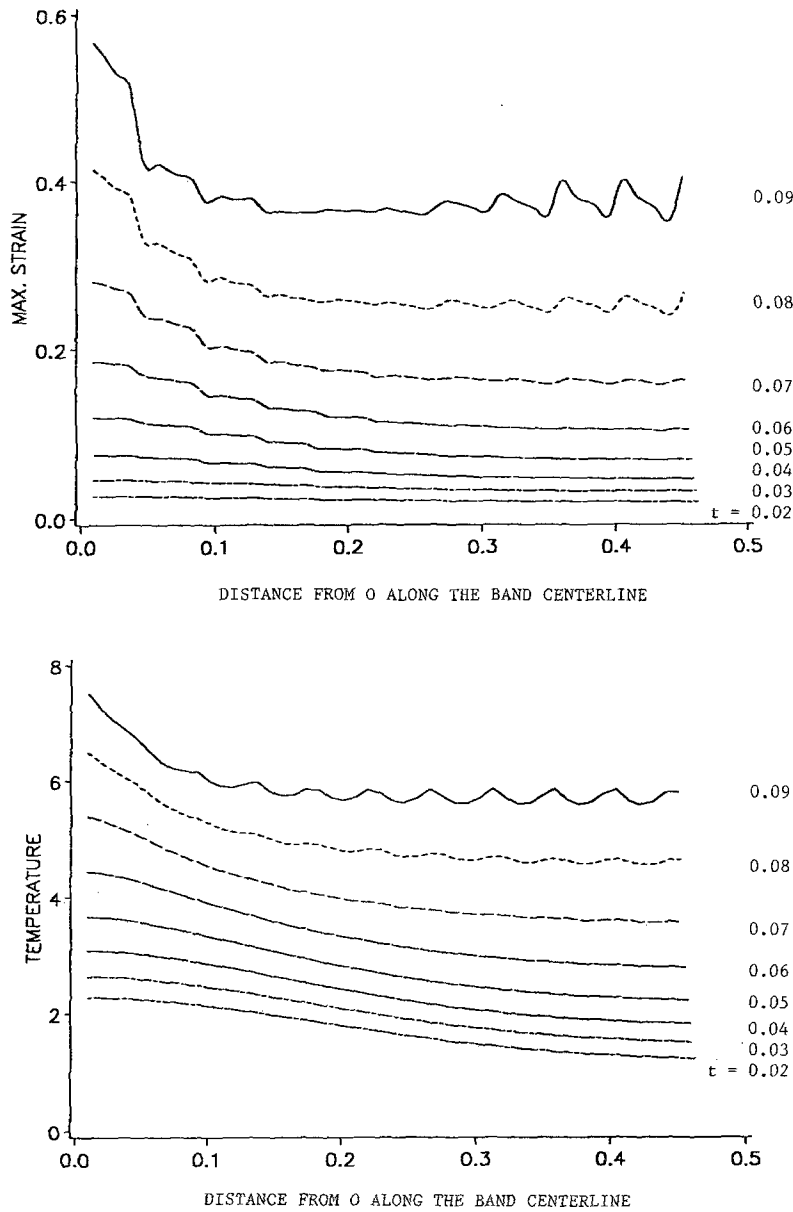


Fig. 6. Variation of the maximum principal logarithmic strain and the temperature along the estimated centerline OEF of the band at different times

block equals one and the block is being compressed at a nondimensional average strain-rate of one after the initial rise to the steady value, the nondimensional vertical displacement of a point on the top surface is slightly less than the nondimensional time. The applied load P is computed by using the relation

$$P = -\int \sigma_{22}(x_1, \bar{x}_2) dx_1,$$

where \bar{x}_2 is the current x_2 -coordinate of a point on the top surface and the limits of integration extend from $x_1 = 0$ to the value of x_1 for points on the right edge. The values of P are significantly

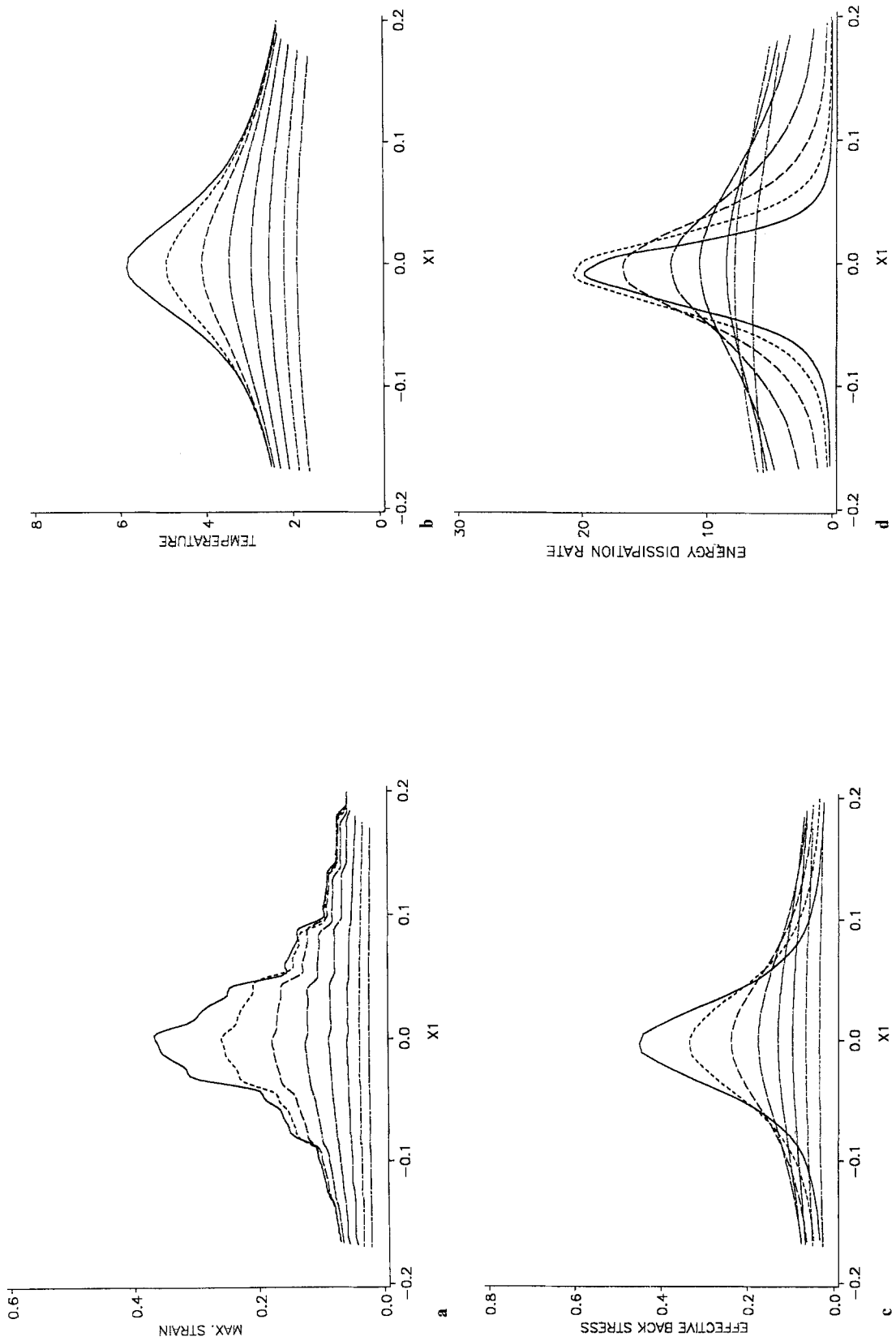


Fig. 7. a-d

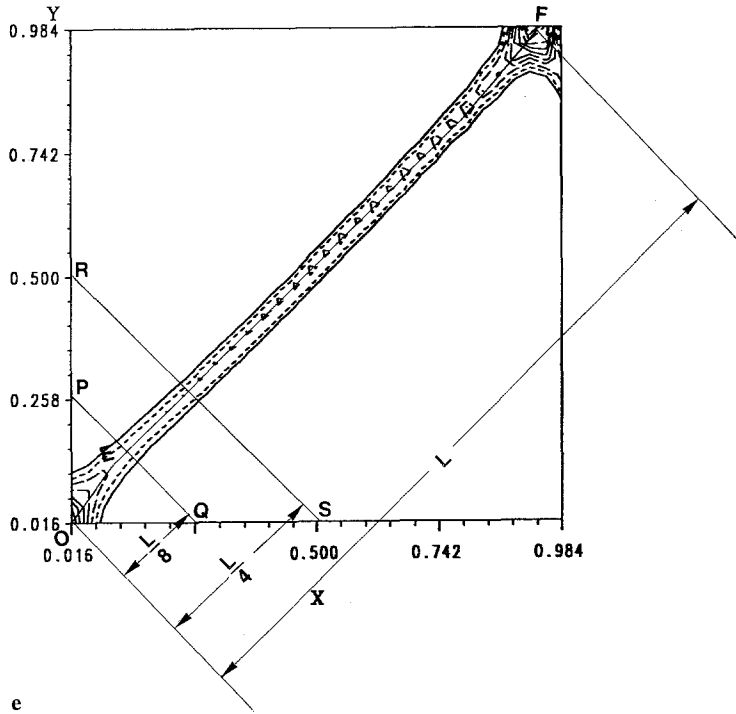


Fig. 7. Distribution at different times, starting with $t = 0.02$, of **a** the maximum principal logarithmic strain, **b** the temperature, **c** the effective back-stress, and **d** the rate of dissipation of the energy density on line PQ . **e** Estimated centerline OEF of the band, and locations of two transverse lines PQ and RS perpendicular to OEF . The curves are for $t = 0.02, 0.03, 0.04, 0.05, 0.06, 0.07, 0.08$, and 0.09

higher than those of the effective stress since the hydrostatic component of the stress tensor and the back-stress make noticeable contributions to the load. The upper set of curves is obtained by assuming that the initial temperature is uniform. Initially, the applied load increases almost linearly in each case due to the linear increase of the applied speed. The heating of the block, because of its plastic deformations, softens it and the load required to deform it decreases. This decrease in the load with increasing compression of the block is more once a shear band has initiated than when there is no band formed. Thus, the development of a shear band results in a decrease in the load carrying capacity of the body. The oscillations in the load displacement curves are probably due to the inertia forces, and can be attributed, at least partially, to the fact that the deformation of the top row of elements is not homogeneous and the computation of tractions at boundary points is less accurate as compared to the solution within the block. It is very likely that the use of a finer mesh would decrease the oscillations in P , but this could not be verified because of the limited computational resources available to us. Also, a finer mesh would improve the resolution of the deformation within the band.

5 Conclusions

We have studied the initiation and growth of a shear band in an elastoviscoplastic body being deformed in plane strain compression at a nominal strain-rate of 5000 sec^{-1} . The effect of inertia forces and the coupling between the thermal and mechanical aspects of the

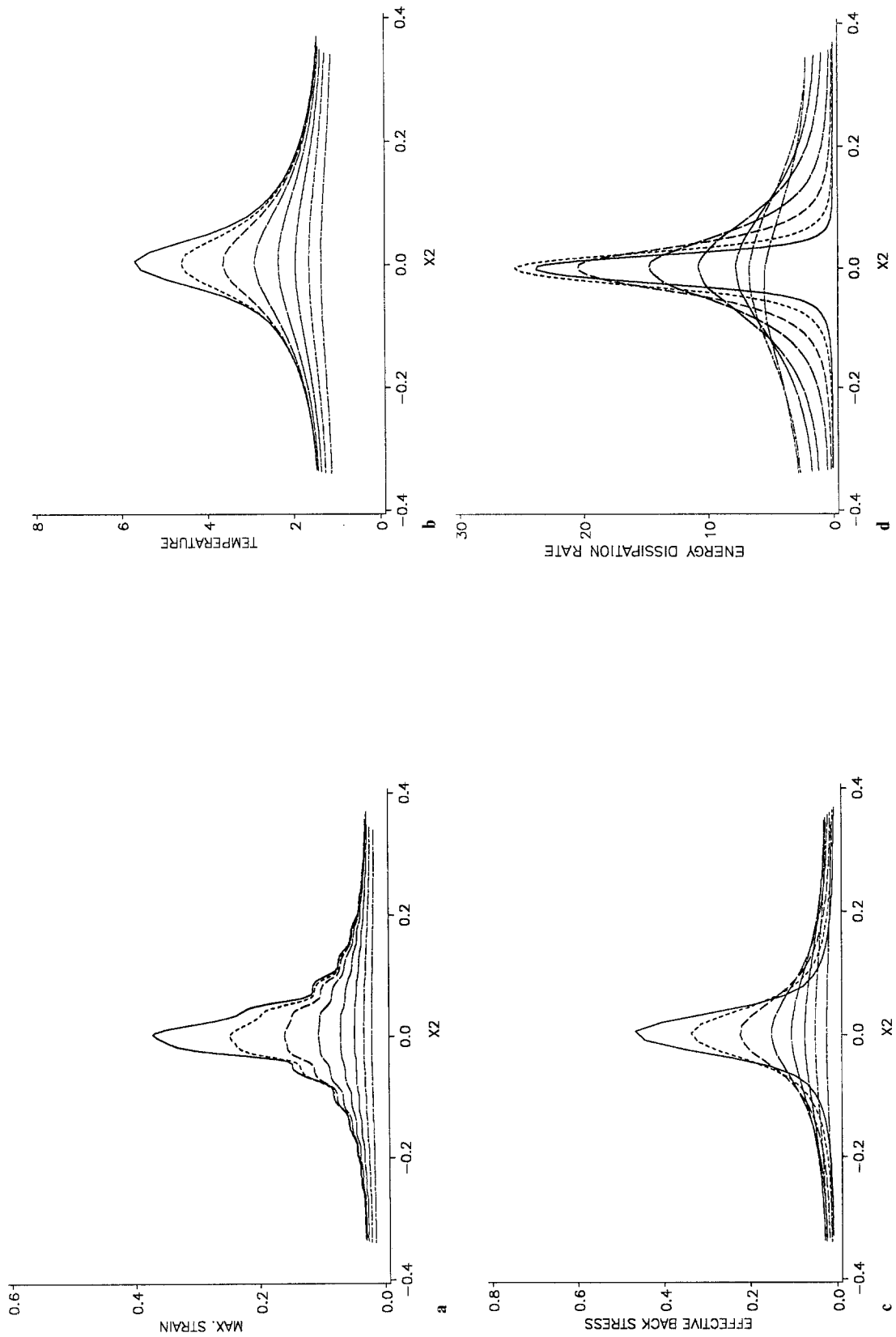


Fig. 8. Distribution at different times of **a** the maximum principal logarithmic strain, **b** the temperature, **c** the effective back-stress, and **d** the rate of dissipation of the energy density on line RS . The curves correspond to $t = 0.02, 0.03, 0.04, 0.05, 0.06, 0.07, 0.08,$ and 0.09

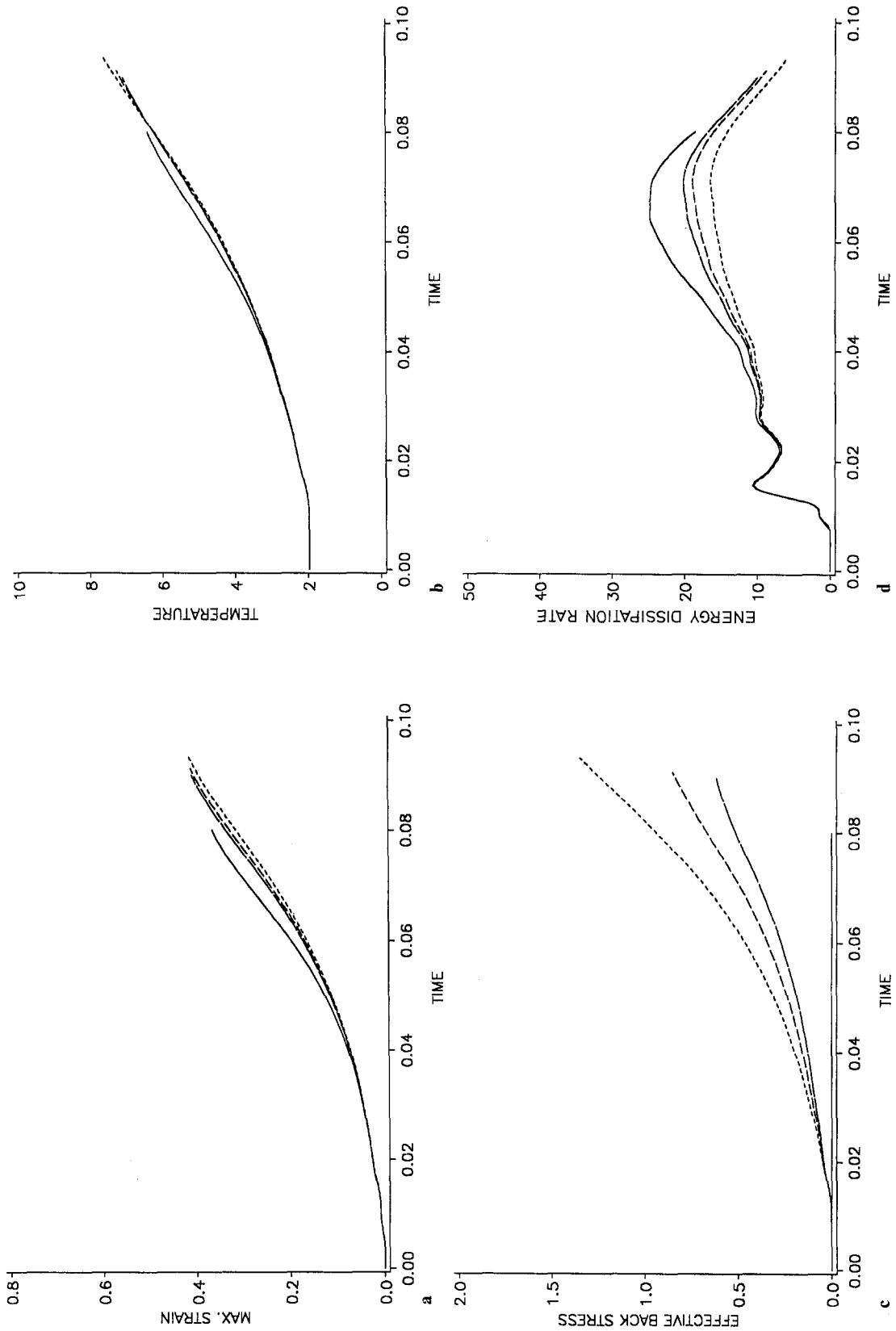


Fig. 9. The evolution of **a** the maximum principal logarithmic strain at $X_1 = X_2 = 0.0066$, **b** the temperature at the origin, **c** the effective back-stress at the origin, and **d** the rate of dissipation of the energy density at the origin. — Case 1, case 4, - - - - case 6, - - - - case 7

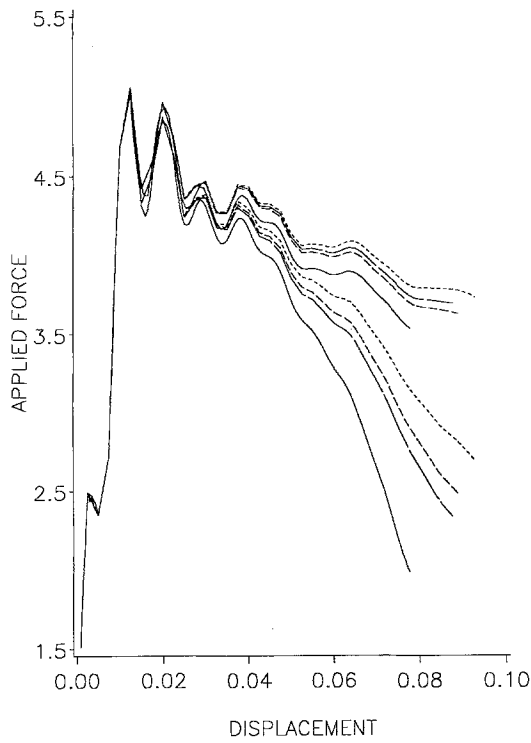


Fig. 10. The load displacement curves for cases 1, 4, 6, and 7. The upper set of curves corresponds to no temperature perturbation. — Case 1, case 4, - - - - case 6, - - - - case 7

deformation is included in the problem formulation and its solution. The effect of texture development on the ensuing deformations is considered by including in the theory two internal variables, a scalar to account for the isotropic hardening of the material and a symmetric traceless second-order tensor to account for the kinematic hardening. The constitutive theory used is due to Anand and his co-workers [4], [5]. The computed results show that the consideration of kinematic hardening does not alter the qualitative nature of results. Also, the results agree qualitatively with those obtained earlier by Batra and co-workers [11], [14], [15], who used a different constitutive relation that does not require the integration with respect to time of the Cauchy stresses, and hence requires fewer computational resources. Because of a lack of test results detailing the evolution of the microstructure within the band in plane strain compression problems, it is not clear which constitutive theory should be used. Also, the determination of the values of material parameters in either theory for high strain-rates and elevated temperatures found within a shear band is still an open problem.

Acknowledgements

This work was supported by the U.S. Army Research Office grant DAAL03-91-G-0084 and the National Science Foundation grant MSS9121279 to the University of Missouri-Rolla. Some of the computations were performed on the NSF sponsored supercomputer center at the Cornell University, Ithaca, NY.

References

- [1] Batra, R. C., Kim, C. H.: Effect of thermal conductivity on the initiation, growth, and band width of adiabatic shear bands. *Int. J. Eng. Sci.* **29**, 949–960 (1991).
- [2] Merzer, A. M.: Modeling of adiabatic shear band development from small imperfection. *J. Mech. Phys. Solids* **30**, 323–338 (1982).
- [3] Dodd, B., Bai, Y.: Width of adiabatic shear bands. *Mat. Sci. Tech.* **1**, 38–40 (1985).
- [4] Anand, L.: Constitutive equations for hot working of metals. *Int. J. Plasticity* **1**, 213–231 (1985).
- [5] Brown, S. B., Kim, K. H., Anand, L.: An internal variable constitutive model for hot working of metals. *Int. J. Plasticity* **5**, 95–130 (1989).
- [6] Tresca, H.: On further application of the flow of solids. *Proc. Inst. Mech. Engrs.* **30**, 301–345 (1878).
- [7] Massey, H. F.: The flow of material during forging. *Proc. Manchester Assoc. Eng.* 21–26 (1921).
- [8] Zener, C., Hollomon, J. H.: Effect of strain-rate on plastic flow of steel. *J. Appl. Phys.* **15**, 22–32 (1944).
- [9] Rogers, H. C.: Adiabatic plastic deformation. *Ann. Rev. Mat. Sci.* **9**, 283–311 (1979).
- [10] Shawki, T., Clifton, R. J.: Shear band formation in thermal viscoplastic materials. *Mech. Mat.* **8**, 13–43 (1989).
- [11] Batra, R. C., Zhu, Z. G.: Dynamic shear band development in a bimetallic body containing a void. *Int. J. Solids Struct.* **27**, 1829–1854 (1991).
- [12] Zbib, H. M., Shawki, T. G., Batra, R. C. (eds.): Material instabilities. *Appl. Mech. Rev.* **45**, 3(2) (1992).
- [13] Hindmarsh, A. C.: ODEPACK — A systematized collection of ODE solvers. In: *Scientific computing* (Stepleman, R. S., et al., eds.). Amsterdam: North-Holland 1983.
- [14] Zhu, Z. G., Batra, R. C.: Dynamic shear band development in plane strain compression of a viscoplastic body containing a rigid inclusion. *Acta Mech.* **84**, 89–107 (1990).
- [15] Batra, R. C., Liu, D. S.: Adiabatic shear banding in plane strain problems. *J. Appl. Mech.* **56**, 527–543 (1989).

Authors' address: Y. M. Wang and R. C. Batra, Department of Mechanical and Aerospace Engineering and Engineering Mechanics, University of Missouri-Rolla, Rolla, MO 65401-0249, U.S.A.